Journal of Power Sources 261 (2014) 175–183

Contents lists available at ScienceDirect

Journal of Power Sources

journal homepage: www.elsevier.com/locate/jpowsour

Effect of cation substitution in the A site on the oxygen semi-permeation flux in $La_{0.5}A_{0.5}Fe_{0.7}Ga_{0.3}O_{3-\delta}$ and $La_{0.5}A_{0.5}Fe_{0.7}Co_{0.3}O_{3-\delta}$ dense perovskite membranes with A = Ca, Sr and Ba (part I)

M. Reichmann [a,d,*], P.-M. Geffroy [a], J. Fouletier [b], N. Richet [c], T. Chartier [a]

[a] SPCTS, CNRS, ENSCI, Université de Limoges, CEC, 12 Rue Atlantis, 87068 Limoges, France
[b] LEPMI, UMR 5279, CNRS – Grenoble INP – Université de Savoie – Université Joseph Fourier, BP 75, 38402 Saint Martin d'Hères, France
[c] Air Liquide, Centre de Recherche Claude-Delorme, 1 chemin de la Porte des Loges, B.P. 126 Les Loges-en-Josas, 78654 Jouy-en-Josas Cedex, France
[d] ADEME, 20, Avenue du Grésillé, B.P. 90406, 49004 Angers Cedex 01, France

HIGHLIGHTS

- The rate determining step of oxygen flux through the membranes is clearly determined.
- The kinetics of oxygen surface exchanges depend on the nature of cation substitution.
- The rate determining step of oxygen flux depends on the temperature.

ARTICLE INFO

Article history:
Received 20 December 2013
Received in revised form
27 February 2014
Accepted 14 March 2014
Available online 27 March 2014

Keywords:
Oxygen surface exchange
Bulk diffusion
Oxygen semi-permeation
Rate determining step

ABSTRACT

Numerous mixed ionic electronic conducting materials with a perovskite structure have been investigated in the literature as potential membrane materials for oxygen separation applications. However, the effect of cation substitution in the A site of a perovskite structure on the oxygen semi-permeation flux is not clearly understood. The goal of this paper is to provide insight into the effect of cation substitution in the A-site on oxygen semi-permeation flux in $La_{0.5}A_{0.5}Fe_{0.7}Ga_{0.3}O_{3-\delta}$ and $La_{0.5}A_{0.5}Fe_{0.7}Co_{0.3}O_{3-\delta}$ perovskite membranes with A = Ca, Sr, and Ba. In addition, the rate-determining step in the trans-membrane oxygen transport was clearly identified based on oxygen diffusion and oxygen surface exchange coefficients for these two perovskite membrane series.

1. Introduction

Oxy-combustion technology is a promising solution for the production of energy with low CO_2 emissions. Indeed, coal is combusted from pure di-oxygen instead of air, allowing for CO_2 capture and storage at a suitable cost. The economic value of oxy-combustion technology is based on pure di-oxygen production at a lower energetic cost compared to typical cryogenic distillation processes. Therefore, oxygen transport membranes (OTM) are an interesting technology for the production of pure di-oxygen [1].

Over the past several years, considerable research has been conducted on new mixed conductor materials for OTM. Mixed ionic–electronic conduction makes it possible to produce pure di-oxygen without external electrodes via oxygen semi-permeation flux through the membrane. Membrane materials with a perovskite structure are of great interest due to their high ionic and electronic conduction properties at high temperature (900 °C) and their good stability under low oxygen partial pressure [2].

The $SrFe_{1-y}Co_yO_{3-\delta}$ perovskite series are well-known membrane materials that exhibit the best oxygen semi-permeation performance [3]. Unfortunately, the chemical stability of this perovskite series under low oxygen partial pressure or CO_2 atmosphere is not sufficient for potential oxy-combustion applications [4,5]. $La_{1-x}Sr_xFe_{1-y}Co_yO_{3-\delta}$ or $La_{1-x}Sr_xFe_{1-y}Ga_yO_{3-\delta}$ perovskite membranes may provide a good compromise between chemical stability and semi-permeation performance.

One of the key parameters for the selection of membrane material and the development of optimal membrane design for industrial applications is rate-determining step (rds) of trans-

* Corresponding author. SPCTS, CNRS, ENSCI, Université de Limoges, CEC, 12 Rue Atlantis, 87068 Limoges, France.
E-mail address: mickael.reichmann@etu.unilim.fr (M. Reichmann).

http://dx.doi.org/10.1016/j.jpowsour.2014.03.074
0378-7753/

membrane oxygen flux. The impact of the nature of the cation in the A-site of a perovskite structure on oxygen bulk diffusion and surface exchange on trans-membrane oxygen flux has rarely been reported in the literature. In this study, a specific apparatus for semi-permeation measurements was used to simultaneously evaluate the oxygen diffusion and surface exchange coefficients of membrane materials and to determine the rate-determining step (rds) in trans-membrane oxygen flux.

The effect of cation substitution in the A-site on the oxygen semi-permeation flux was investigated for the $La_{0.5}A_{0.5}Fe_{0.7}Ga_{0.3}O_{3-\delta}$ and $La_{0.5}A_{0.5}Fe_{0.7}Co_{0.3}O_{3-\delta}$ perovskite series (with A = Ba, Ca and Sr). The aim was to evaluate the effect of cation substitution in the A-site on oxygen transport mechanisms through the membrane (e.g., oxygen diffusion and surface exchange at the membrane surface). In a future study, the effect of cation substitution in the B-site on the oxygen semi-permeation flux will be investigated for a wide range of perovskite membrane compositions.

2. Experimental

2.1. Powder synthesis

$La_{0.5}A_{0.5}Fe_{0.7}Ga_{0.3}O_{3-\delta}$ and $La_{0.5}A_{0.5}Fe_{0.7}Co_{0.3}O_{3-\delta}$ perovskite powders (with A = Ba, Ca and Sr) are synthesized using a solid–solid route. High purity oxide and carbonate precursors including La_2O_3 (99.99%, Sigma Aldrich), Ga_2O_3 (99.99%, Sigma Aldrich), Fe_2O_3 (99.5%, Alfa Aesar), Co_3O_4 (99.7%, Alfa Aesar), $CaCO_3$ (99.9%, Alfa Aesar), $BaCO_3$ (99.95%, Alfa Aesar) and $SrCO_3$ (99.99%. Alfa Aesar) are mixed by attrition using 800 μm zirconia balls in ethanol media (600 rpm, 3 h). The obtained powder is calcined at 1000 °C for 8 h. The phase purity is confirmed with X-ray diffraction (Siemens D5000). The calcined powders are ground by attrition milling (1000 rpm) to obtain a monomodal grain size of approximately 1–2 μm.

2.2. Shaping using tape casting process, firing and density measurements

A tape casting process is used to obtain thin pellets (150 μm thick). Then, the pellets are thermo-laminated at 60 °C under 50 MPa and fired to obtain a relative density of more than 95% and a thickness of 1 mm. The sintering conditions for the membrane materials are listed in Table 1. More details regarding sample shaping are provided in previous studies [6,7]. The density of the fired membrane is controlled with the Archimedes method, and the grain size is evaluated using a scanning electron microscope (SEM Cambridge Instruments).

2.3. Oxygen surface exchange and semi-permeation measurements

The oxygen semi-permeation and oxygen activities at the membrane surface are measured using a homemade apparatus, as described in previous studies [8,9] and shown in Fig. 1. The dense membrane is sealed between two alumina tubes with the use of gold rings to avoid surfaces contaminations [10]. The

Table 1
Sintering conditions and chemical compositions of the membrane materials.

Membrane materials	Acronym	Sintering conditions
$La_{0.5}Sr_{0.5}Fe_{0.7}Ga_{0.3}O_{3-\delta}$	LSFG	1350 °C, 4 h, air
$La_{0.5}Sr_{0.5}Fe_{0.7}Co_{0.3}O_{3-\delta}$	LSFCo	1350 °C, 4 h, air
$La_{0.5}Ca_{0.5}Fe_{0.7}Ga_{0.3}O_{3-\delta}$	LCFG	1250 °C, 4 h, air
$La_{0.5}Ca_{0.5}Fe_{0.7}Co_{0.3}O_{3-\delta}$	LCFCo	1250 °C, 4 h, air
$La_{0.5}Ba_{0.5}Fe_{0.7}Co_{0.3}O_{3-\delta}$	LBFCo	1150 °C, 4 h, air

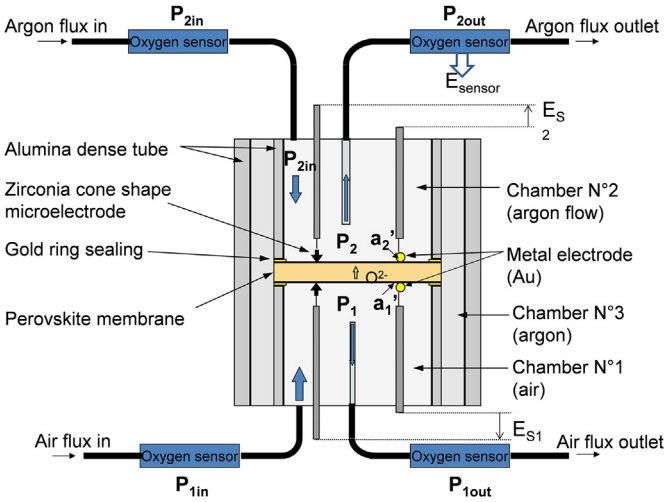

Fig. 1. Oxygen semi-permeation apparatus [8].

measurements are performed at a temperature ranging from 980 °C to 600 °C with an interval of 25 °C with an air/argon atmosphere gradient. The oxygen enrichment on the argon side is measured using a YSZ–oxygen sensor. On the surface membrane, the oxygen surface activities are measured using pure ionic conductor tips (in ZrO_2–8%Y_2O_3) and a metallic electrode in contact with the surface membrane. Then, the oxygen chemical potential through the membrane is evaluated, as previously described by Geffroy et al. [8].

The electromotive force, E_{sensor}, is provided by the YSZ–oxygen sensors used to measure the oxygen pressure in the argon flux outlet, P_{2out}, following the Nernst law:

$$E_{sensor} = \frac{RT}{4F}\ln\frac{P_{2out}}{P_{O_2(air)}} \quad (1)$$

where R, T and F are the universal gas constant, the temperature in Kelvins, and the Faraday constant, respectively. $P_{O_2(air)}$ (with $P_{O_2(air)} = 0.21 \approx P_1 = P_{1out} \approx P_{1in}$), and P_2 (with $P_2 = P_{2out}$), correspond to the oxygen partial pressure in air and the oxygen pressure in the argon flowing upstream or downstream in the experimental setup, respectively.

E_{s1} and E_{s2} correspond to the electromotive forces caused by the variation in di-oxygen activity between the inlet gas and the oxygen-rich and lean surfaces of the membrane, respectively. These two values are calculated from the Nernst law as follows:

$$E_{s1} = \frac{RT}{4F}\ln\frac{a_1}{a_1'} = \frac{\Delta\mu_{O_2}^{surf(ox)}}{4F} \quad (2)$$

$$E_{s2} = \frac{RT}{4F}\ln\frac{a_2'}{a_2} = \frac{\Delta\mu_{O_2}^{surf(red)}}{4F} \quad (3)$$

where a_1 is the di-oxygen activity in air and is equal to the oxygen partial pressure, P_1. Here, P_1, P_{1in} and P_{1out} are equal to 0.21. a_1' is the di-oxygen activity at the oxygen-rich surface of the membrane. a_2 is the di-oxygen activity in argon gas near the oxygen-lean surface and is equal to P_{2out}. We also assumed that the P_{2out} of the gas outlet from the argon chamber corresponds to P_{2out} near the membrane surface. a_2' is the di-oxygen activity on the oxygen-lean surface of the membrane.

$\Delta\mu_{O_2}^{surf\ (ox)}$ and $\Delta\mu_{O_2}^{surf\ (red)}$ are the gradients of the di-oxygen activity potential on the oxygen-rich and oxygen-lean surfaces of the membrane, respectively.

2.4. Measurement of electrical conductivity

The electrical conductivity is evaluated by a four probe device from room temperature to 1000 °C under air. The bar samples are obtained using a tape casting process and sintered using similar conditions as reported in Table 1. After sintering, the bar samples have approximate dimensions of 1 × 2.5 × 24 mm^3. Both ends of the bar sample were coated by platinum electrodes. Two additional platinum electrodes were placed 5–8 mm from each end of the bar. The platinum electrodes were prepared via platinum ink coating (Pt paste Ferro, CDS), and the sample was heated to 1000 °C in air to obtain cohesive and porous platinum electrodes.

3. Results and discussion

3.1. Densification and phase purity

All of the sintered membranes have a relative density larger than 94%, except for $La_{0.5}Ba_{0.5}Fe_{0.7}Ga_{0.3}O_{3-\delta}$ (LBFG). Different thermal treatments have been performed to obtain a dense LBFG membrane, but the relative density of the LBFG material remains low, or the samples are cracked. Therefore, the LBFG material was not further investigated here.

Table 2
Relative density of the perovskite membrane series.

Acronym	Mean grain size	Density of the starting powder (pycnometer)	Relative density of the sintered membrane
LSFG	2–4 μm	5.70 g cm^{-3}	>95%
LSFCo	4–10 μm	6.10 g cm^{-3}	>95%
LCFG	Low crystallinity	5.70 g cm^{-3}	95%
LCFCo	1–2 μm	5.54 g cm^{-3}	94%
LBFCo	1–4 μm	6.06 g cm^{-3}	>95%

The SEM micrographs (Fig. 2) show the microstructure of the sintered materials. The mean grain sizes are very similar (i.e., approximately 2–4 μm, Table 2), except for the LSFCo membrane, which had a larger grain size of approximately 4–10 μm. We assume that this low variation in grain size does not affect the oxygen semi-permeation flux. The LCFG membrane exhibits a very low crystallization degree without apparent grains. This low

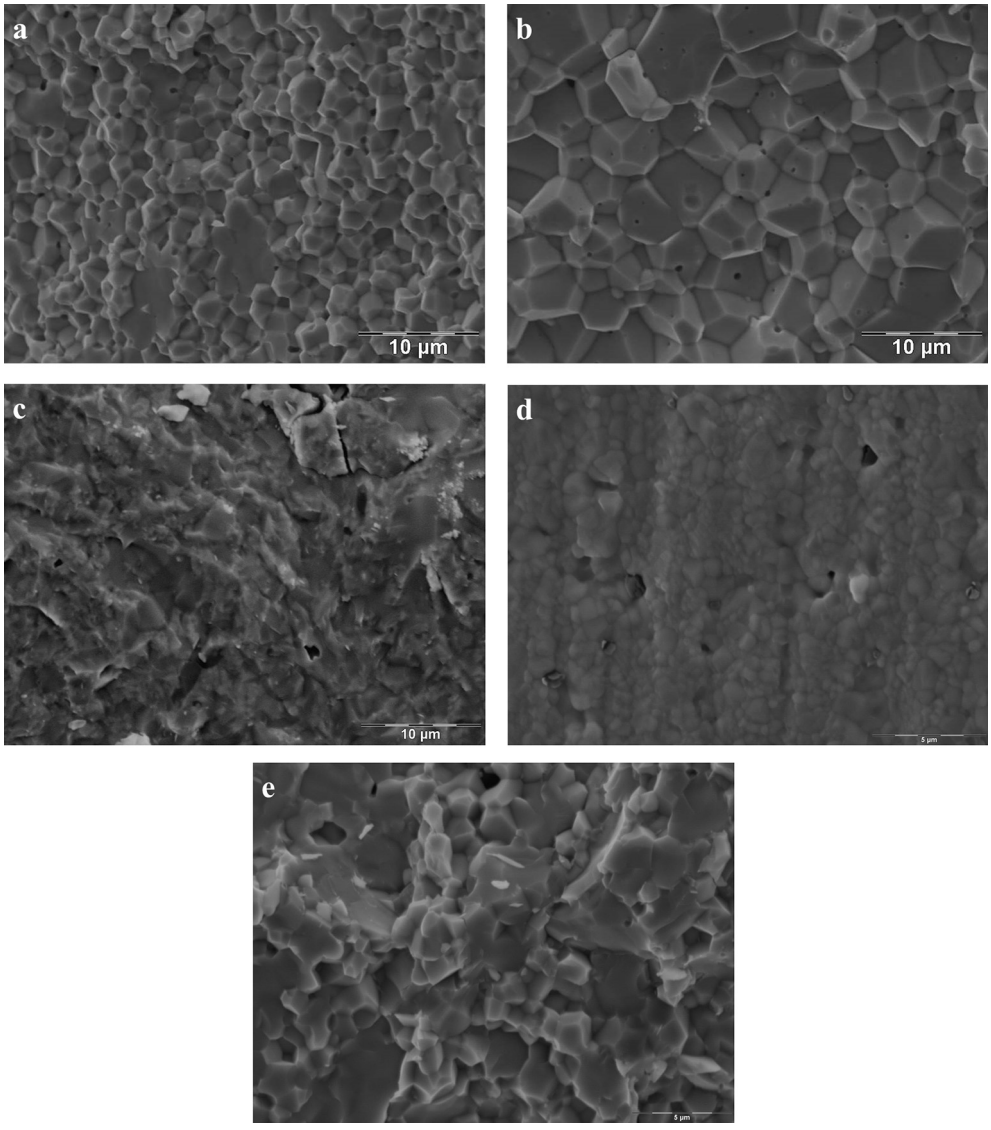

Fig. 2. SEM micrographs of the a) LSFG, b) LSFCo, c) LCFG, d) LCFCo and e) LBFCo membranes.

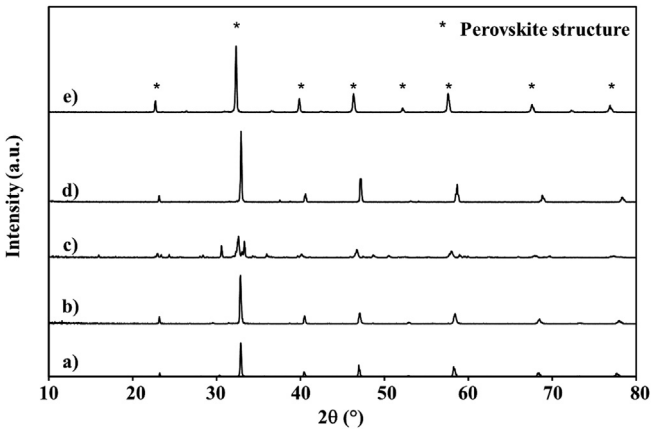

Fig. 3. XRD diagrams of the a) LSFG, b) LSFCo, c) LCFG, d) LCFCo and e) LBFCo membranes.

crystallization degree in the LCFG membranes most likely disfavors a high oxygen diffusion coefficient and high oxygen semi-permeation flux.

Fig. 3 shows the X-ray diffraction diagrams for the sintered membrane series. All of the sintered membrane materials correspond to a well-defined perovskite structure after sintering with few secondary phases, except for the LCFG material. For the LCFG membrane, the perovskite phase corresponds to a minor phase and the membrane material is not well crystallized, as indicated by the SEM micrographs.

3.2. Oxygen semi-permeation fluxes

Fig. 4 shows the oxygen flux through the membranes at 600–970 °C. All of the oxygen fluxes exhibit the same order of magnitude (6–23 × 10^{-4} mol m^{-2} s^{-1}), except for the LCFG membrane. The oxygen flux in the LCFG membrane is one order of magnitude lower than the other materials. The low oxygen flux through the LCFG membrane (6 × 10^{-5} mol m^{-2} s^{-1}) is most likely due to low crystallization of the perovskite membrane material after sintering (Fig. 2). Surprisingly, the nature of the substitution cation exhibits little impact on the oxygen semi-permeation flux through the membrane materials that have a similar microstructure.

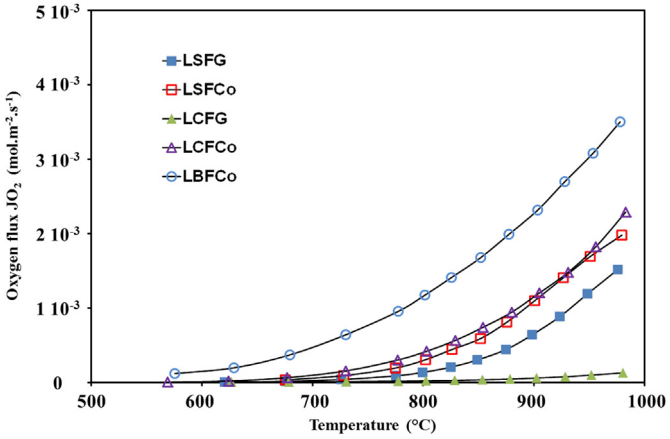

Fig. 4. Oxygen semi-permeation flux through the $La_{0.5}A_{0.5}Fe_{0.7}Ga_{0.3}O_{3-\delta}$ and $La_{0.5}A_{0.5}Fe_{0.7}Co_{0.3}O_{3-\delta}$ perovskite membrane series (with A = Ba, Ca and Sr).

The oxygen fluxes in the LSFG, LSFCo and LCFCo membranes are very similar, whereas the oxygen flux in the LBFCo membrane is slightly higher. The oxygen flux through the $La_{0.5}A'_{0.5}Co_{0.3}Fe_{0.7}O_{3-\delta}$ membranes slightly increases in the following order Ba > Ca > Sr. This trend is in good agreement with the results reported by Teraoka et al. [11] for $La_{0.6}A'_{0.4}Co_{0.8}Fe_{0.2}O_{3-\delta}$ materials.

3.3. Identification of the rate determining step for the oxygen flux

Fig. 5 shows the Arrhenius plots for the oxygen semi-permeation flux, and Table 3 provides the activation energies of the oxygen semi-permeation flux through all of the perovskite membranes. The Arrhenius plot shows two slopes corresponding to two rate-determining steps (rds) in the oxygen semi-permeation flux (i.e., one at a low temperature between 700 and 900 °C and the other one at a high temperature above 900 °C).

At low temperatures (between 700 and 900 °C), the activation energy (Ea) of the oxygen flux depends on the nature of the substitution cation in the A-site (i.e., Ea(Ba) ≈ 80 kJ mol^{-1}, Ea(Ca) ≈ 115 kJ mol^{-1}, Ea(Sr) ≈ 150 kJ mol^{-1}). These Ea values are in good agreement with oxygen semi-permeation fluxes obtained for cobaltite material membranes. A similar trend was reported by Tsai et al. for $La_{0.4}A_{0.6}Fe_{0.8}Co_{0.2}O_{3-\delta}$ perovskite materials [12] (Ea(Ba) = 72.38 ± 0.75 kJ mol^{-1}, Ea(Ca) = 95.33 ± 0.94 kJ mol^{-1} between 780 °C and 980 °C, Ea(Sr) = 105.61 ± 3.83 kJ mol^{-1} between 825 °C and 915 °C). However, the Ea values reported by Tsai et al. correspond to intermediate Ea values at the low and high temperatures calculated in this work because these authors considered only one mechanism of oxygen transport from 825 to 915 °C. Unfortunately, this temperature range corresponds to a mixed regime for the $La_{0.4}A_{0.6}Fe_{0.8}Co_{0.2}O_{3-\delta}$ perovskite membrane (or the intersection between two slopes on the Arrhenius plots).

The Ea values calculated at high temperatures are lower than those calculated at low temperatures, except for the LCFG membrane. This behavior is due to the evolution of a predominant rate-determining step in the trans-membrane oxygen flux. For example, we recently demonstrated that the oxygen flux in the $La_2NiO_{4+\delta}$ membrane was governed by oxygen surface exchange at low temperatures (<900 °C) and by bulk diffusion at high temperatures (>1000 °C) [9].

Therefore, the Ea values for the Co-based materials at low (below 800 °C) and high temperatures (up to 900 °C) correspond to the surface exchange and oxygen bulk diffusion mechanisms, respectively (i.e., Ea(surface exchange) ≈ 110–150 kJ mol^{-1} and Ea(bulk diffusion) ≈ 70–80 kJ mol^{-1}). Xu et al. [13] also observed two slopes for the Arrhenius plots of oxygen flux for a similar

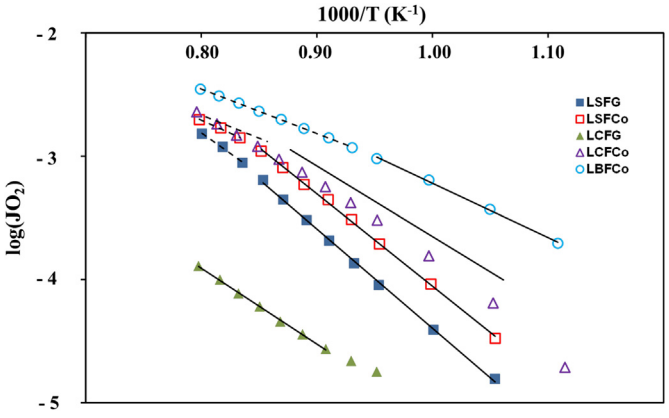

Fig. 5. Arrhenius plot of oxygen semi-permeation fluxes.

Table 3
Activation energy values at low and high temperatures for cobaltite and gallate perovskite membrane series.

Materials series	Cation nature	Membrane materials	Ea (kJ mol^{-1}) 700–900 °C	Ea (kJ mol^{-1}) 900–1000 °C
LAFCo	Sr	LSFCo	144	81
	Ca	LCFCo	107	69
	Ba	LBFCo	80 (700–825 °C)	68 (825–1000 °C)
LAFGa	Sr	LSFG	154	128
	Ca	LCFG	118	118
	Ba	LBFG	Not measured	Not measured

membrane material (i.e., $La_{0.6}Sr_{0.4}Fe_{0.8}Co_{0.2}O_{3-\delta}$ with Ea = 191 kJ mol^{-1} at low temperatures and Ea = 115 kJ mol^{-1} at high temperatures). This slight discrepancy between the Ea values reported in our work and by Xu et al. is most likely due to the difference in the experimental conditions (i.e., membrane thickness, oxygen partial pressure, and microstructure of membrane materials). However, the temperature range corresponding to a mixed regime reported by Xu (or the intersection between two slopes observed on the Arrhenius plots) are similar (i.e., from 800 to 900 °C).

The large variation in the Ea values can be easily correlated to the evolution of the rds identified here via B_c coefficient as a function of $1/T$ (Fig. 6). B_c is a new criterion introduced by Geffroy et al. [14], which is defined in Eq. (4):

$$B_e = \frac{\Delta\mu_{O_2}^{surface}}{\Delta\mu_{O_2}^{bulk}} \quad (4)$$

According to Eq. (4), three cases can be considered:

- when $B_c > 1$, the oxygen flux is governed by oxygen surface exchange.
- when $B_c < 1$, the oxygen flux is governed by oxygen diffusion.
- when $B_c \approx 1$, a mixed regime is present in which the oxygen flux is governed by both oxygen diffusion and surface exchange.

The B_c value corresponds to the ratio between the drop of oxygen chemical potential through the bulk and at the membrane surface. Then, we can discriminate between the oxygen transport mechanism linked to oxygen surface exchange at the membrane face in contact with air or in contact with argon atmosphere using two values: B_c^{rich} and B_c^{lean}, respectively. Fig. 6 shows that the oxygen flux is predominantly governed by oxygen bulk-diffusion mechanism at high temperatures and by surface exchange at low temperatures, especially for the LSFG membranes. In addition, we assume that there is an intermediary range of temperatures corresponding to a mixed regime (when B_c is close to unity), where the oxygen flux is governed by both mechanisms for trans-membrane oxygen transport. This range of temperatures corresponding to the mixed regime depends on the membrane materials.

For the LSFG perovskite membrane, the variation in the Ea value with temperature is linked to the evolution of B_c. Indeed, the B_c^{lean} value below 900 °C is larger than unity, and the oxygen flux is predominantly governed by oxygen surface exchange at the oxygen lean membrane face. However, the B_c^{lean} value quickly decreases with temperature, and B_c^{lean} is close to unity when the temperature is higher than 950 °C, which means that the oxygen flux is governed by a mixed regime at high temperatures (up to 950 °C). We observe a similar trend but to a lesser extent for the LCFCo membrane.

For the LCFG and LBFCo membranes, no variation in the Ea is observed between 600 and 1000 °C because the oxygen flux is governed by oxygen bulk diffusion in this temperature range. The Ea value is larger than that determined for the cobaltite perovskite materials. This high Ea value results in low crystallization of the perovskite phase or a low oxygen diffusion coefficient for the LCFG material.

Fig. 6a clearly shows the influence of the substitution cation in the A-site for the LAFCo perovskite membrane on the nature of the rds. At low temperatures (<900 °C), oxygen flux through LAFCo membranes is governed by oxygen surface exchange when A = Ca, by a mixed regime when A = Sr and by oxygen bulk diffusion when

Table 4
Type of rate determining step (rds) with the corresponding B_c^{rich} and B_c^{lean} values.

Values of B_c^{rich} and B_c^{lean}	Type of the rds	Corresponding domain in Fig. 8
B_c^{rich} and $B_c^{lean} < 1$	Bulk diffusion	A
B_c^{rich} and $B_c^{lean} \approx 1$	Mixed regime: bulk and surface(s)	B
$B_c^{rich} >> B_c^{lean}$ and $B_c^{rich} > 1$	Oxygen rich surface	C
$B_c^{rich} << B_c^{lean}$ and $B_c^{lean} > 1$	Oxygen lean surface	D
$B_c^{rich} \approx B_c^{lean} > 1$	Oxygen rich and lean surfaces	E

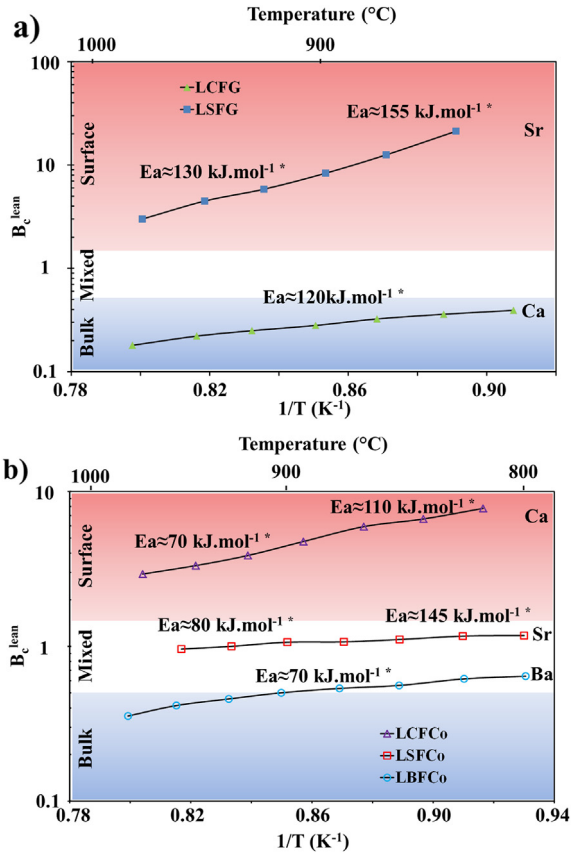

Fig. 6. Evolution of the rate-determining step for oxygen semi-permeation flux as a function of temperature for the a) cobaltite membranes and b) gallate membranes. *: Ea are calculated from Fig. 5.

Table 5
Values of the different parameters used to calculate D_O, k^{rich}, k^{lean} and k^{lean}.

900 °C	δ_{air}	δ_{argon}	V_m (Å^3)	C_O^{rich} (mol cm^{-3})	C_O^{lean} (mol cm^{-3})
LCFCo	0.11	0.22	58.13	8.26×10^{-2}	7.94×10^{-2}
LSFCo	0.16	0.32	58.10	8.12×10^{-2}	7.66×10^{-2}
LBFCo	0.13	0.25	61.27	7.79×10^{-2}	7.44×10^{-2}
LCFG	0.09	0.17	60.39	8.02×10^{-2}	7.78×10^{-2}
LSFG	0.15	0.30	58.21	8.13×10^{-2}	7.70×10^{-2}

A = Ba. However, the B_c^{lean} coefficients decrease quickly when the temperature increases, and the Ea of the oxygen flux is very close at high temperatures. Indeed, the nature of the substitution cation in the A-site has a large impact on the kinetics of oxygen surface exchanges at the LAFCo membrane surface (predominant rds at low temperatures), but a small impact on the oxygen diffusion coefficient of LAFCo perovskite materials (predominant rds at high temperatures), as reported in Table 5.

3.4. Profiles of oxygen chemical potential

The profiles of the oxygen chemical potential (μ_{O_2}) through the perovskite membranes at 900 °C are shown in Fig. 7. These profiles easily allow us to determine the rate-determining step in oxygen flux. For the $La_{0.5}A_{0.5}Fe_{0.7}Co_{0.3}O_{3-\delta}$ perovskite materials, the values of μ_{O_2} that decrease through the membrane are similar (between 36 and 43 kJ mol^{-1}, Fig 7b, d and e). Nonetheless, three cases can be distinguished where oxygen flux is governed by a mixed regime (LSFCo, Fig. 7b), by surface exchange on the oxygen lean face (LCFCo, Fig 7d), or by bulk diffusion (LBFCo, Fig. 7e). The nature of the cation in the A-site of the perovskite structure has a substantial effect on the rds of oxygen flux through the membrane.

The drop of oxygen chemical potential through the LSFG membrane (Fig. 7a) is larger than that observed through the LAFCo membrane (i.e., 47 kJ mol^{-1} and near 40 kJ mol^{-1}, respectively), which is due to a large drop of oxygen chemical potential at the oxygen lean face ($\Delta\mu_{O_2}^{surf(ox)}$(LSFG) = 35 kJ mol^{-1}). In contrast, a large oxygen chemical potential drop through the LCFG membrane (Fig. 7c) results from a large gradient in the oxygen chemical potential through the membrane bulk ($\Delta\mu_{O_2}^{bulk} = 52$ kJ mol^{-1}), which is due to the low degree of crystallization or low oxygen ionic conductivity of the LCFG membrane.

Fig. 8 shows the evolution of the B_c^{lean} and B_c^{rich} values (and corresponding rds in the oxygen flux) relative to the membrane material and temperature. Table 4 lists the different rds in the oxygen flux with the corresponding values of B_c^{lean} and B_c^{rich}.

3.4.1. Value of B_c at 900 °C

No membranes are located in C and E-domain, in Fig. 8, at 900 °C. It means that oxygen surface exchange on oxygen-rich face is never the rate-determining step in the oxygen flux. The LCFG and

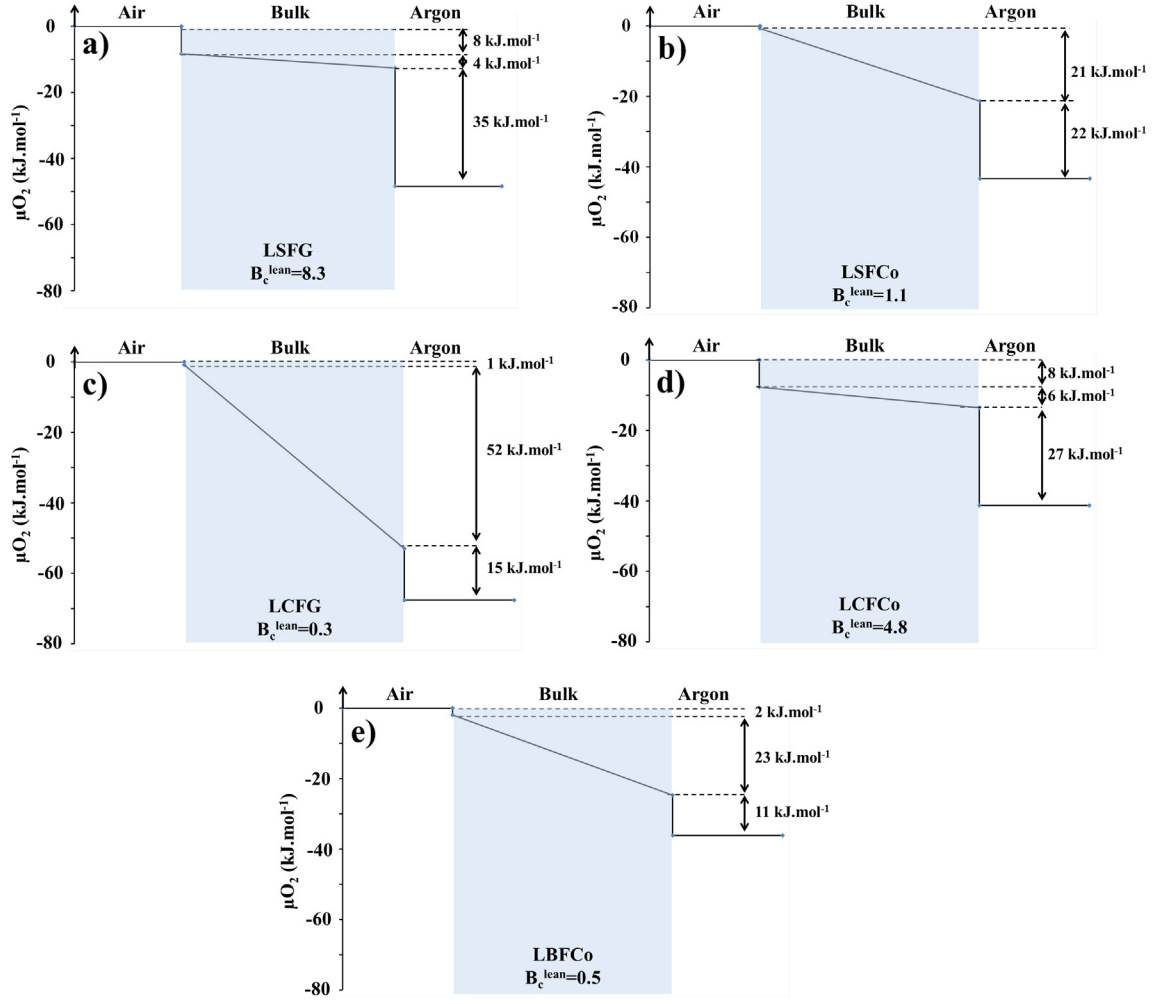

Fig. 7. Profiles of the oxygen chemical potential through the a) LSFG, b) LSFCo, c) LCFG, d) LCFCo and e) LBFCo membranes at 900 °C.

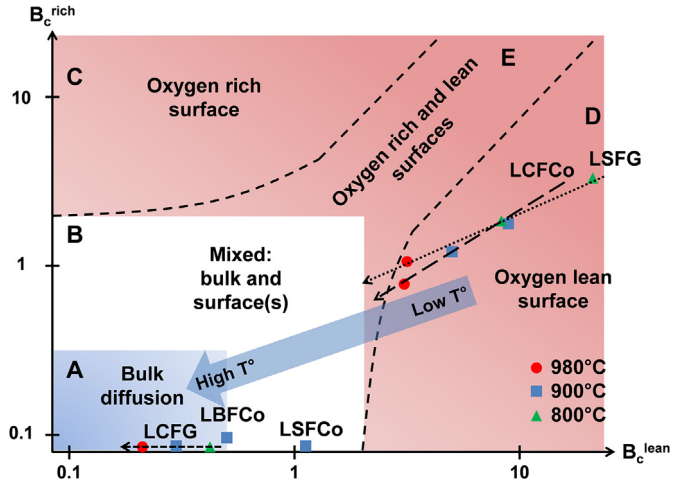

Fig. 8. Evolution of the rate determining steps in trans-membrane oxygen transport relative to temperature and membrane materials.

LBFCo membranes are located in A-domain, where the semi-permeation flux is governed by oxygen bulk-diffusion transport.

B_c^{lean} value of LSFCo membrane is close to unity corresponding to mixed regime where the oxygen flux is governed by oxygen surface exchange at oxygen-lean face and oxygen bulk diffusion. In the case of LCFCo and LSFG membranes, the surface exchange at oxygen-lean face limits the oxygen semi-permeation flux (D-domain in Fig. 8).

The nature of cation in A-site has an important effect on the rds in oxygen semi-permeation flux. For instance, the oxygen fluxes obtained with LSFCo and LCFCo membranes are very close, although B_c^{lean} values are very different, 1.05 and 5, respectively. However, it is not possible to establish a clear correlation between the rds and the nature of cation in A-site.

3.4.2. Evolution of the rate determining step with the temperature

Fig. 8 indicates that the B_c^{lean} values decrease with the temperature. At low temperatures, the oxygen flux tends to be predominantly governed by oxygen surface exchanges, while at high temperatures, the oxygen flux tends to be predominantly governed by oxygen bulk diffusion. For example, in the LCFG membrane, oxygen flux is only governed by oxygen bulk diffusion from 800 to 900 °C, while the oxygen flux is governed by surface exchange for the LCFCo and LSFG membranes from 800 to 980 °C.

Indeed, the surface exchange kinetics are very low at a low temperature and quickly increase with temperature because the activation energy of this mechanism is larger than that of the oxygen bulk diffusion. Therefore, the oxygen bulk diffusion is often the rds for oxygen flux at high temperatures (up to 1000 °C in some cases).

3.5. Surface exchanges and diffusion coefficients

The coefficient of diffusion, D_O, is defined thank to the Wagner's model in Eq. (5):

$$D_O = \frac{4RTLJ_{O_2}}{C_O \Delta\mu_{O_2}^{bulk}} \quad (5)$$

The formalism concerning the surface exchange coefficients have been described by Kim et al. [15] in Eqs. (6)–(9). It is necessary to distinguish two kinds of surface exchange coefficients k and K. K correspond to the surface exchange coefficient, independent from the oxygen partial pressure in gas, whereas k corresponds to the usual surface exchange coefficient depending on oxygen partial pressure in gas.

$$k^{rich} = \frac{2J_{O_2}}{C_O^{rich}\left(\exp\left(\frac{n\mu_{O_2}^{gas\ (ox)}}{RT}\right) - \exp\left(\frac{n\mu_{O_2}^{surf\ (ox)}}{RT}\right)\right)} \times \left(\frac{P_1^{out}}{P_{O_2}^{air}}\right)^n \quad (6)$$

$$k^{lean} = \frac{2J_{O_2}}{C_O^{lean}\left(\exp\left(\frac{n\mu_{O_2}^{surf\ (red)}}{RT}\right) - \exp\left(\frac{n\mu_{O_2}^{gas\ (red)}}{RT}\right)\right)} \times \left(\frac{P_2^{out}}{P_{O_2}^{air}}\right)^n \quad (7)$$

$$K^{rich} = \frac{2J_{O_2}}{C_O^{rich}\left(\exp\left(\frac{n\mu_{O_2}^{gas\ (ox)}}{RT}\right) - \exp\left(\frac{n\mu_{O_2}^{surf\ (ox)}}{RT}\right)\right)} \quad (8)$$

$$K^{lean} = \frac{2J_{O_2}}{C_O^{lean}\left(\exp\left(\frac{n\mu_{O_2}^{surf\ (red)}}{RT}\right) - \exp\left(\frac{n\mu_{O_2}^{gas\ (red)}}{RT}\right)\right)} \quad (9)$$

It is possible to link the two coefficients with the simple relation expressed in Eq. (10):

$$k = K \times \left(\frac{P^{out}}{P_{O_2}^{air}}\right)^n \quad (10)$$

In these equations, C_O^{rich} and C_O^{lean} are the oxygen molar concentration at the oxygen rich and lean surface respectively, given in Table 5, L is the thickness of the membrane, and n is typically equal to 0.5 for MIEC materials. C_O is estimated thank to the relation $C_O = (3-\delta)/V_m$, with δ the oxygen over-stoichiometry amounts in the perovskite structure, determined by thermogravimetry method and V_m the molar volume estimated from crystalline parameters obtained by X-ray diffraction. In D_O calculation, C_O is the average of C_O^{rich} and C_O^{lean} values, because D_O is considered to be constant in the bulk membrane.

$\mu_{O_2}^{gas(ox)}$ and $\mu_{O_2}^{gas(red)}$ are the oxygen chemical potentials in air and argon, respectively. For example, $\mu_{O_2}^{gas(ox)} = RT\ln(P_1^{out}/P_{O_2}^{air})$

Table 6
Fundamental parameters including oxygen diffusion (D_O), surface exchange coefficient at oxygen rich (k^{rich}) and lean (K^{lean} and k^{lean}) face, ionic conductivity (σ_i) and electronic conductivity (σ_e) for cobaltite and gallate perovskite membranes materials investigated in this study.

900 °C		D_O (cm^2 s^{-1})	$k^{rich} = K^{rich}$ (cm s^{-1})	K^{lean} (cm s^{-1})	k^{lean} (cm s^{-1})	σ_i (S cm^{-1})	σ_e (S cm^{-1})
Materials series	Composition						
LAFCo	LCFCo 5573	1.1×10^{-6}	9.9×10^{-6}	8.7×10^{-6}	1.0×10^{-6}	33×10^{-2}	141
	LSFCo 5573	2.7×10^{-7}	1.0×10^{-4}	1.3×10^{-5}	1.2×10^{-6}	8×10^{-2}	326
	LBFCo 5573	4.4×10^{-7}	6.4×10^{-5}	5.0×10^{-5}	7.9×10^{-6}	13×10^{-2}	7
LAFGa	LCFG 5573	6.0×10^{-9}	3.5×10^{-6}	4.4×10^{-6}	1.4×10^{-7}	0.2×10^{-2}	30
	LSFG 5573	7.3×10^{-7}	4.6×10^{-6}	1.4×10^{-5}	1.2×10^{-6}	22×10^{-2}	97

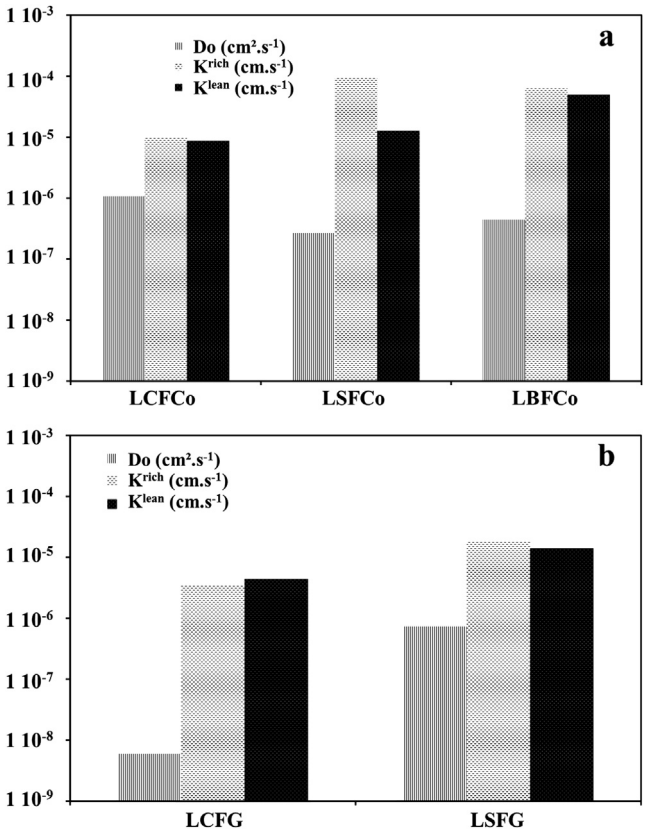

Fig. 9. Fundamental parameters including oxygen diffusion (D_O), surface exchange coefficient at oxygen rich (K^{rich}) and lean (K^{lean}) face at 900 °C for a) cobaltite and b) gallate perovskite membranes materials investigated in this study.

with $P_{O_2}^{air}$ as the reference pressure corresponding to the oxygen partial pressure in air.

$\mu_{O_2}^{surf(ox)}$ and $\mu_{O_2}^{surf(red)}$ are the oxygen chemical potentials on oxidizing and reducing surfaces, respectively.

K^{rich} and K^{lean} correspond to coefficient surface exchanges on feed and permeate sides, respectively.

In this way, we distingue two coefficients of oxygen surface exchange. K coefficients corresponds to oxygen surface exchange coefficients normalized for $P_{O_2} = 0.21$, which could be independent on the oxygen partial pressure in gas, and *k* coefficients is the usual oxygen surface exchange coefficients depending on oxygen partial pressure in gas. Then, the values of *K* coefficients are more relevant for a comparison of intrinsic oxygen surface exchange kinetics on different membrane materials.

On the oxygen side, $P_1^{out} \approx P_{O_2}^{air} \approx 0.21$, the surface exchange coefficient becomes $k^{rich} = K^{rich}$.

The surface exchange coefficients and the coefficient of bulk diffusion are listed in Table 6 and presented in Fig. 9. The oxygen coefficient diffusion and surface exchanges at 900 °C are calculated from the semi-permeation measurements.

For the predominant electronic conductors ($\sigma_e >> \sigma_i$), the ionic conductivity can be estimated using semi-permeation measurements and the Nernst–Einstein relationship (Eq. (11)):

$$\sigma_i = \frac{16F^2 L J_{O_2}}{\Delta\mu_{O_2}^{bulk}} \quad (11)$$

From electrical measurements, it is possible to determine the ionic transport number of the membrane materials.

D_O coefficients (or ionic conductivity) are very similar for all of the materials (2.7–11 10^{-7} cm^2 s^{-1}) except for the LCFG membrane (5.9 10^{-9} cm^2 s^{-1}), which is most likely due to the low degree of crystallization of the material (Table 6 and Fig. 9). For the $La_{0.4}Ba_{0.6}Fe_{0.8}Co_{0.2}O_{3-\delta}$ perovskite membrane, Diethelm et al. [16] report a similar coefficient of diffusion and ionic conductivity (i.e., $D_O = 5.5$ 10^{-7} cm^2 s^{-1} and $\sigma_i = 0.15$ S cm^{-1}). For the $La_{0.6}Sr_{0.4}Fe_{0.8}Co_{0.2}O_{3-\delta}$ membrane with a 3–5 μm grain sized microstructure, Zeng et al. [17] report an ionic conductivity of 0.065 S cm^{-1}, which is in good agreement with the values obtained in this work. However, the value of K^{rich} appears to be overestimated and must be equal to about 2 10^{-5} cm^2 s^{-1}. The ionic conductivity measured for the LSFG 5573 membrane is larger than that measured by Kharton et al. [18] for the $La_{0.4}Sr_{0.6}Fe_{0.6}Ga_{0.4}O_{3-\delta}$ membrane (i.e., 0.22 S cm^{-1} and 0.08 S cm^{-1}, respectively). The results found by Geffroy et al. [19] are very similar of us for the $La_{0.6}Sr_{0.4}Fe_{0.6}Ga_{0.4}O_{3-\delta}$ membrane with $D_O = 4\ 10^{-7}/7.2\ 10^{-7}$ cm^2 s^{-1}, $K^{rich} = 2\ 10^{-5}/4.6\ 10^{-6}$ cm s^{-1} and $K^{lean} = 3\ 10^{-5}/1.4\ 10^{-5}$ cm s^{-1} at 900 °C (Table 6).

Co-based materials exhibit a higher surface exchange coefficient than Ga-based ones, especially at the oxygen lean face (one order of magnitude higher). These high surface exchange coefficients lead to high fluxes for the $La_{0.5}A_{0.5}Fe_{0.7}Co_{0.7}O_{3-\delta}$ materials. For the cobaltite membranes, the surface exchange coefficients increase in the following order: Ba > Sr > Ca.

4. Conclusions

The effect of cation substitution in the A site of a perovskite structure on the different mechanisms in trans-membrane oxygen transport has been clearly identified in this study using a specific apparatus that allows for measurement of the oxygen activity at both membrane faces. These oxygen activity measurements at both membrane faces led to the identification of the rate-determining step in trans-membrane oxygen using new criteria: B_c^{rich} and B_c^{lean} values.

The partial cation substitution in the A site with Ca, Sr and Ba indicated that the nature of the cation in the A site has a large impact on the oxygen diffusion and surface exchange coefficients of the perovskite materials. The La substitution by Ba corresponds to membrane materials with higher coefficients of oxygen diffusion and surface exchange. In addition, the rds in the trans-membrane oxygen flux depends on the temperature and membrane materials.

Indeed, the nature of both cations in the A site and B site has a significant impact on the kinetics of oxygen surface exchange, and the coefficient of surface exchange. A similar approach can be suggested to better understand cation substitution in the B site of a perovskite structure. The results from this study will be reported in the future.

Acknowledgments

The authors wish to express their gratitude to the French Environment and Energy Management Agency (ADEME) for financial support of this work.

References

[1] U. Balachandran, J.T. Dusek, R.L. Mieville, R.B. Poeppel, M.S. Kleefisch, S. Pei, T.P. Kobylinski, C.A. Udovich, A.C. Bose, Appl. Catal. A 133 (1995) 19–29.
[2] P.M. Geffroy, J. Fouletier, N. Richet, T. Chartier, Chem. Eng. Sci. 87 (2013) 408–433.
[3] Y. Teraoka, H.-M. Zhang, S. Furukawa, N. Yamazoe, Chem. Lett. (1985) 1743–1746.
[4] W. Chen, C. Chen, L. Winnubst, Solid State Ionics 196 (2011) 30–33.
[5] J. Yi, S. Feng, Y. Zuo, W. Liu, C. Chen, Chem. Mater. 17 (2005) 5856–5861.
[6] A. Julian, E. Juste, P.M. Geffroy, V. Coudert, S. Degot, P. Del Gallo, N. Richet, T. Chartier, J. Membr. Sci. 333 (2009) 132–140.

[7] P.M. Geffroy, J.M. Bassat, A. Vivet, S. Fourcade, E. Juste, A. Julian, T. Chartier, P. Del Gallo, N. Richet, J. Membr. Sci. 354 (2010) 6–13.
[8] P.M. Geffroy, A. Vivet, J. Fouletier, N. Richet, P. Del Gallo, T. Chartier, J. Electrochem. Soc. 158 (2011) B971–B979.
[9] P.M. Geffroy, M. Reichmann, T. Chartier, J.-M. Bassat, J.-C. Grenier, J. Membr. Sci. 451 (2014) 234–242.
[10] A. Vivet, P.M. Geffroy, V. Coudert, J. Fouletier, N. Richet, T. Chartier, J. Membr. Sci. 366 (2011) 132–138.
[11] Y. Teraoka, T. Nobunaga, N. Yamazoe, Chem. Lett. (1987) 503–506.
[12] C.Y. Tsai, A.G. Dixon, Y.H. Ma, W.R. Moser, M.R. Pascucci, J. Am. Ceram. Soc. 81 (1998) 1437–1444.
[13] S.J. Xu, W.J. Thomson, Chem. Eng. Sci. 54 (1999) 3839–3850.
[14] P.M. Geffroy, A. Vivet, J. Fouletier, C. Steil, E. Blond, N. Richet, P. Del Gallo, T. Chartier, J. Electrochem. Soc. 160 (2013) F60–F68.
[15] S. Kim, Y.L. Yang, A.J. Jacobson, B. Abeles, Solid State Ionics 121 (1999) 31–36.
[16] S. Diethelm, J. Van herle, Solid State Ionics 174 (2004) 127–134.
[17] P.Y. Zeng, R. Ran, Z.H. Chen, H.X. Gu, Z.P. Shao, J.C. Diniz da Costa, J. Membr. Sci. 302 (2007) 171–179.
[18] V.V. Kharton, A.L. Shaulo, A.P. Viskup, M. Avdeev, A.A. Yaremchenko, M.V. Patrakeev, A.I. Kurbakov, E.N. Naumocih, F.M.B. Marques, Solid State Ionics 150 (2002) 229–243.
[19] P.M. Geffroy, H. Yang, A. Vivet, T. Chartier, G. Dezanneau, J. Electrochem. Soc. 161 (2014) F1–F8.